

1 **Mining ancient microbiomes using selective enrichment of damaged DNA**
2 **molecules**

3 Clemens L. Weiß^a, Marie-Theres Gansauge^b, Ayinuer Aximu-Petri^b, Matthias Meyer^b,
4 Hernán A. Burbano^{a#}

5 ^aResearch Group for Ancient Genomics and Evolution, Department of Molecular
6 Biology, Max Planck Institute for Developmental Biology, 72076 Tübingen, Germany

7 ^bDepartment of Evolutionary Genetics, Max Planck Institute for Evolutionary
8 Anthropology, 04103 Leipzig, Germany

9 Running Head: Uracil selection for validation of ancient metagenomes

10 #Address correspondence to Hernán A. Burbano, hernan.burbano@tuebingen.mpg.de

11 **Abstract**

12 The identification of bona fide microbial taxa in microbiomes derived from historical
13 samples is complicated by the unavoidable mixture between DNA from ante- and
14 post-mortem microbial colonizers. One possibility to distinguish between these sources
15 of microbial DNA is querying for the presence of age-associated degradation patterns
16 typical of ancient DNA (aDNA). The presence of uracils, resulting from cytosine
17 deamination, has been detected ubiquitously in aDNA retrieved from diverse sources,
18 and used as an authentication criterion. Here, we employ a library preparation method
19 that separates molecules that carry uracils from those that do not for a set of samples
20 that includes Neandertal remains, herbaria specimens and archaeological plant
21 remains. We show that this method facilitates the discovery of authentic ancient
22 microbial taxa, as it amplifies degradation patterns that would otherwise be difficult to
23 detect in sequences from diverse microbial mixtures.

24 **Importance**

25 The utility of DNA from historical specimens is being recognized in a growing number of
26 fields, ranging from human, animal and plant genetics, to microbiology and
27 epidemiology of infectious diseases. Providing positive evidence for the authenticity of
28 such ancient DNA from diverse sources is instrumental for all studies that make use of
29 this resource. This is especially challenging when studying ancient microbes, due to
30 their high genetic diversity and the incompleteness of reference databases. The method

31 we employ and characterize here aids this process through the selective enrichment of
32 molecules that carry signatures of age-associated degradation.

33 **Introduction**

34 DNA retrieved from historical or ancient samples is a complex mixture of
35 molecules that contains not only endogenous host DNA, but also DNA from
36 microorganisms that were present ante-mortem or that colonized the tissue post-mortem
37 (1). Therefore, all ancient DNA (aDNA) shotgun sequencing projects are metagenomic
38 in nature. While earlier aDNA research has mostly focused on the evolution of animals
39 and plants (2, 3), a growing number of studies are now centering on the identification
40 and characterization of ancient pathogens and microbiomes (4). Ancient microbes
41 permit the replacement of indirect inferences about the past with direct observations of
42 microbial genomes through time. In the pathogen field, it has been possible to identify
43 causal and/or associated agents of historical plant and animal disease outbreaks, as
44 well as their spreading patterns throughout both space and time (e.g. (5, 6)). Another
45 challenging endeavour is the characterization of shifts in composition of microbial
46 communities over time. For example, dental calculus from hominids has been exploited
47 as a source of ancient microbiomes and analyzed in the context of diet and lifestyle
48 changes (7–9), whereas coprolites have been used to investigate ecological interactions
49 between animals and microorganisms (10). However, this approach is at its beginnings

50 and the influence of major selective pressures on microbiome evolution remains to be
51 explored.

52 A major challenge for the study of aDNA in general, and ancient microbiomes in
53 particular, is the presence of contaminating exogenous DNA, which makes distinction
54 between *bona fide* ancient microbiome sequences and those of recent origin crucial.
55 One of the most typical features of aDNA is the presence of uracils (Us) that originate
56 from post-mortem deamination of cytosines (Cs), especially in single-stranded
57 overhangs at molecule ends (11). Uracils are read as thymines (Ts) by most DNA
58 polymerases, which generates a characteristic increase in C-to-T substitutions at the
59 end of aDNA sequences ((11), Figure 1D and 2A). The presence of such C-to-T
60 substitutions can be used as evidence for the authenticity of DNA sequences retrieved
61 from historical material (12–14).

62 Recently, a single-stranded library preparation method (U-selection) was
63 developed, which allows physical separation of uracil-containing molecules from
64 non-deaminated ones (15). In U-selection all library molecules are initially immobilized
65 on streptavidin beads, to which molecules without uracils remain attached (U-depleted
66 fraction), while uracil-containing molecules (originally deaminated) are released into
67 solution (U-enriched fraction). U-selection was originally developed with the aim of
68 increasing the amount of ancient hominid DNA (e.g. Neandertals) from a background of
69 present-day human and microbial DNA (15). However, the method seems to be
70 specially suited to study microbiomes, due to the inherent difficulty to authenticate their

71 ancient origin. This complication arises from the fact that microbes can colonize tissues
72 at different times, resulting in different levels of deamination of microbial DNA in
73 historical samples. Although sequences that carry terminal C-to-T substitutions can be
74 selected *in silico* (16, 17), there are two factors that could hinder this approach. Firstly,
75 low levels of deamination will reduce the number of molecules suitable for selection *in*
76 *silico*. Secondly, high sequence divergence between samples and reference genomes
77 can mask age-associated deamination signals thereby hinder authentication..
78 Consequently, enriching for deaminated molecules during library preparation is
79 fundamental to tackling these problems. As a proof-of-principle experiment, we used
80 here U-selection in combination with taxonomic binning of Illumina sequenced reads to
81 characterize the microbiomes of Neandertal bones (~39,000 years old), herbaria
82 specimens (between 41 and 279 years old) and plant archaeological remains (~2,000
83 years old) (Table 1).

84 **Table 1.** Provenance of herbarium specimens and archaeological remains

ID	Country of origin	Age	Species	Reference*
KM177500	UK	171 ⁺	<i>Solanum tuberosum</i>	1
KM177497	UK	170 ⁺	<i>Solanum tuberosum</i>	1
BM000815937	UK	279 ⁺	<i>Solanum lycopersicum</i>	2
BH0000061459	USA	119 ⁺	<i>Arabidopsis thaliana</i>	3
OSU13900	USA	82 ⁺	<i>Arabidopsis thaliana</i>	4
NY1365364	USA	127 ⁺	<i>Arabidopsis thaliana</i>	5
NY1365375	USA	119 ⁺	<i>Arabidopsis thaliana</i>	5
CS5	USA	1852 ⁺⁺	<i>Zea mays</i>	6
CS6	USA	Undated	<i>Zea mays</i>	6
CS20	USA	1881 ⁺⁺	<i>Zea mays</i>	6
El Sidrón 1253	Spain	39,000 ⁺⁺	Neanderthal	7
Vindija 33.17	Croatia	Undated	Neanderthal	8
Vindija 33.19	Croatia	Undated	Neanderthal	8

85 *¹Kew Royal Botanical Gardens; ²Natural History Museum, London; ³Cornell Bailey
86 Hortorium; ⁴Ohio State University Herbarium; ⁵New York Botanical Garden;
87 ⁶Turkey Pen Shelter, UTAH, USA; ⁷El Sidrón Cave, Spain; ⁸Vindija Cave, Croatia.

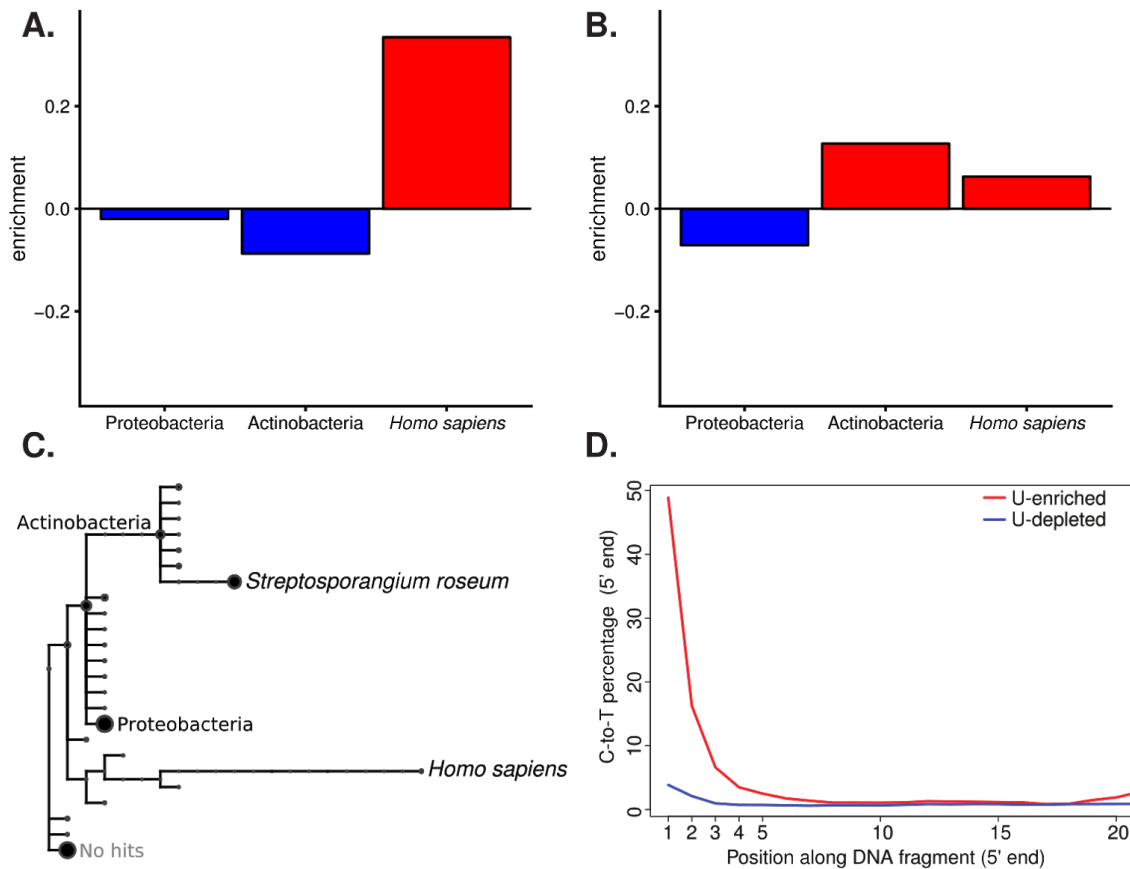
88 ⁺Calculated from collection dates (in years).

89 ⁺⁺B.P. (Before present years)

90 **Results and Discussion**

91 Our experiments were motivated by the previous observation that in some
92 Neandertal samples, e.g. from El Sidrón, Spain, the proportion of Neandertal DNA
93 fragments remains unchanged in both the U-depleted and U-enriched fractions,
94 whereas in others, from Vindija Cave, Croatia, this proportion increased in the
95 Uracil-enriched fraction (15). It was hypothesized that the latter effect could have been

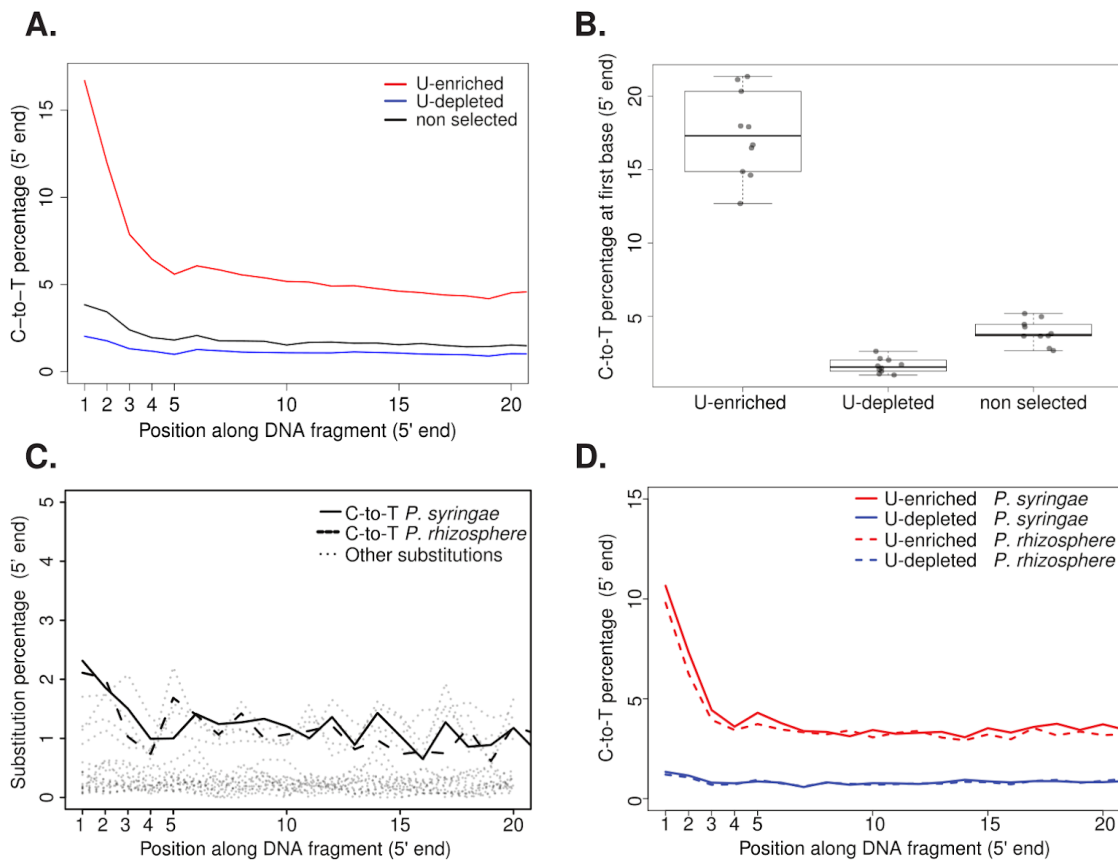
96 due to differences in deamination, and hence in age, between Neandertal- and
97 microbial-derived DNA fragments. To explore this effect further, we re-analyzed the
98 previously generated Neanderthal sequence data from both sites by performing
99 taxonomic binning of reads derived from the U-depleted and U-enriched fractions,
100 instead of aligning them only to the human reference genome, as had been done
101 previously. Reads aligning to the two most abundant bacterial phyla (Actinobacteria and
102 Proteobacteria) from the Vindija Neandertals were enriched in the U-depleted fraction,
103 while hominid reads were enriched in the U-enriched fraction (Figure 1A). This is in
104 accordance with a previous study that reported absence of DNA damage in
105 Actinobacteria derived from a Neandertal bone from Vindija cave (18). In contrast, in
106 reads obtained from the El Sidrón Neandertals, we found enrichment of both hominid
107 and Actinobacteria reads in the U-enriched fraction, whereas Proteobacteria reads were
108 enriched in the U-depleted fraction. (Figure 1B). Overall, bacteria-derived reads were
109 dominated by the Actinobacteria *Streptosporangium roseum* (Figure 1C), which showed
110 almost 50% deamination at the first base in the U-enriched fraction (Figure 1D),
111 suggesting its ancient origin. The analysis of reads derived from Neandertal bones
112 illustrates how U-selection permits distinguishing between ancient bacteria enriched in
113 the U-enriched fraction and more recent colonizers enriched in the U-depleted fraction.



114 **Figure 1.** Relative enrichment, taxonomic assignment and substitution profiles of
115 Neandertal-derived U-selected libraries. **A.** Relative enrichment (number of reads)
116 in the U-enriched relative to the U-depleted fraction from Vindija Neandertal
117 assigned to the phyla Actinobacteria and Proteobacteria, as well as to *Homo*
118 *sapiens*. **B.** Relative enrichment (number of reads) in the U-enriched relative to
119 the U-depleted fraction from Sidrón Neandertal assigned to the phyla
120 Actinobacteria and Proteobacteria, as well as to *Homo sapiens*. **C.** Taxonomic tree
121 of reads from Sidrón Neandertal assigned to different taxonomic levels. The size
122 of the circle represents the amount of reads assigned to a particular part or the
123 taxonomy. Assignments to the phyla Actinobacteria and Proteobacteria, as well as
124 the species *Streptosporangium roseum* and *Homo sapiens* are named in the
125 taxonomic tree. **D.** Cytosine to Thymine substitutions at the 5' end of reads aligned
126 to *S. roseum* from the Sidrón Neandertal U-selected library (U-enriched and
127 U-depleted fractions).

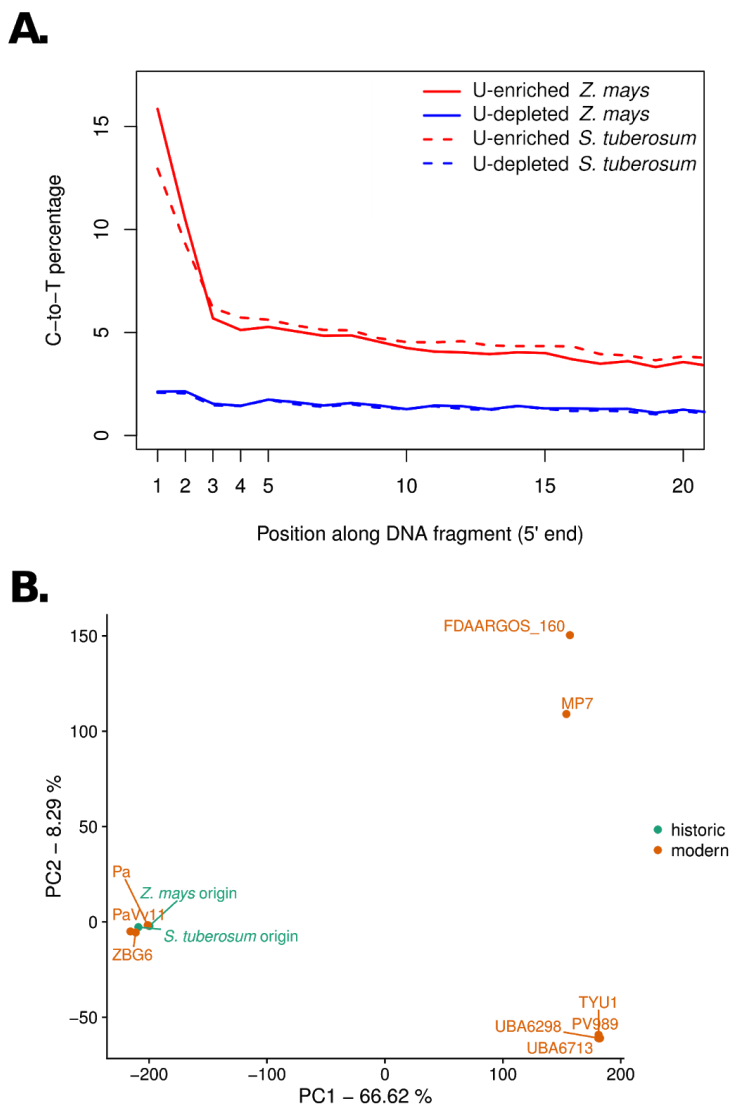
128 In order to further evaluate the performance of U-selection in characterizing
129 microbial communities, we selected a set of plant samples (both herbaria specimens
130 and archaeological remains) with low levels of deamination. We extracted DNA from
131 plant samples and generated libraries using both a regular double-stranded (ds)
132 approach (19), and U-selection (15). Sequences from the dsDNA libraries were then
133 used as a baseline to evaluate depletion and enrichment of uracil-containing molecules
134 (Figure 2A). U-selection successfully enriched for deaminated molecules in all plant
135 samples, as it is manifest in the much higher levels of deamination present in the
136 U-enriched fraction compared with the dsDNA libraries and the U-depleted fraction
137 (Figure 2A-B). The plant samples showed substantial variation in the content of
138 endogenous DNA (2.8-91%), which was very similar between the U-depleted and
139 U-enriched fractions, indicating similar levels of deamination between host- and microbe
140 derived reads (Figure S1A). Assuming that plant- and microbial-derived DNA deaminate
141 at a similar rate (20), this observation indicates that microbes found in plant tissue were
142 present at the time of collection or colonized the tissue shortly thereafter. The
143 percentage of reads (including host-derived reads) that could be taxonomically binned
144 varied depending on the sample (Figure S1B) and, since the host genome was included
145 in the nucleotide database, positively correlated with the percentage of host
146 endogenous DNA (Figure S1C). The inability to taxonomically assign the vast majority of
147 reads from samples with low endogenous DNA reflects the incompleteness of the
148 reference database compared to the diversity of the microbiomes in those samples.

149 Additionally, single stranded DNA library preparation methods as employed during Uracil
150 enrichment generate shorter reads (21, 22), which are more difficult to map to a
151 reference genome and to assign taxonomically to a nucleotide database. This is
152 reflected in the higher percentage of reads mapped and assigned from the dsDNA
153 library compared with shorter reads derived from both the U-depleted and U-enriched
154 fraction (Figure S2A-B). Originally, it was reported that the U-enriched fraction shows a
155 mild increase in GC-content (15), however in the plant libraries analyzed here we did not
156 find a significant difference in GC-content between the U-depleted and U-enriched
157 fractions (Figure S2C). In theory, since Us originate from Cs, the U-enriched fraction
158 would be enriched for GC-rich species and GC-rich genomic regions within a given
159 genome. However, as the enrichment would depend on the diversity of taxa present and
160 their relative age difference, and hence difference in deamination, GC-biases, if any, are
161 expected to be highly sample-dependent.



162 **Figure 2.** Patterns of cytosine to thymine (C-to-T) substitutions at the 5' end of
163 plant- and *Pseudomonas*-derived reads. **A.** C-to-T substitutions at the 5' end of
164 *Solanum tuberosum* sample KM177500 for a non-selected and U-selected library
165 (U-enriched and U-depleted fractions). **B.** Distributions of C-to-T substitution
166 percentage at first base (5' end) for non-selected and U-selected libraries
167 (U-enriched and U-depleted fractions). Median values are denoted as black lines
168 and points show the original value for each individual sample. **C.** Substitution
169 patterns at the 5' end of *Pseudomonas syringae* and *Pseudomonas rhizosphere*
170 mapped reads from a non-selected library from a *Solanum tuberosum* sample
171 KM177500. **D.** Cytosine to Thymine substitutions at the 5' end of *P. syringae* and
172 *P. rhizosphere* mapped reads from a U-selected library (U-enriched and
173 U-depleted fractions) from a *Solanum tuberosum* sample KM177500.

174 Given the low taxonomic diversity of microorganisms in the samples included in
175 our proof-of-principle experiment, instead of centering our analyses on the
176 compositional assessment of microbial communities, we investigated in detail samples
177 in which a specific microbe or group of microbes were more prevalent based on read
178 abundance. We identified a large number of reads that were assigned to the bacterium
179 *Pantoea vagans* in a potato (*Solanum tuberosum*) and a maize (*Zea mays*) sample
180 (Figure S3). In both samples we found patterns of C-to-T substitutions that suggest the
181 historical nature of the sequenced reads (Figure 3A). Since *P. vagans* is a plant epiphyte
182 (23), it is not entirely surprising to find it in two different plant species. We compared the
183 potato and maize *P. vagans* with publicly available genomes using single nucleotide
184 polymorphisms (SNPs) ascertained in these modern samples. Our analysis linked the
185 two historical strains to a distinct cluster of modern strains based on genetic similarity
186 (Figure 3B). Based on a set of 432,891 SNPs, the two historical isolates showed 95%
187 SNP identity between them, and an average of 92% SNP identity between historical and
188 modern strains of the same cluster. Conversely, comparisons between historical strains
189 and any modern strain of a different cluster showed only an average of 59% identity at
190 variable positions.



191 **Figure 3.** Substitution patterns and genetic distances of the bacterium *Pantoea*
192 *vagans* identified from *Zea mays* and *Solanum tuberosum* samples (same
193 samples as in Figure S3). **A.** Cytosine to Thymine substitutions at the 5' end of *P.*
194 *vagans* for U-selected libraries (U-enriched and U-depleted fractions) from *Z.*
195 *mays* and *S. tuberosum*. **B.** Principal component analysis of *P. vagans* from *Z.*
196 *mays* and *S. tuberosum* samples, as well as nine publicly available genomes,
197 based on single nucleotide polymorphisms. Numbers in axis labels indicate the
198 percentage of the variance explained by each principal component (PC).

199 In a potato sample, in which the pathogenic oomycete *Phytophthora infestans*
200 was previously identified (6), we found a large portion of reads assigned to the bacterial
201 genus *Pseudomonas*. Reads were assigned in particular to the species *Pseudomonas*
202 *syringae* and *Pseudomonas rhizosphere* in different proportions (Figure S4). We
203 performed de novo assembly using reads assigned to the genus *Pseudomonas* and
204 aligned the contigs to the reference genomes of *P. syringae* and *P. rhizosphere* covering
205 about 80% of both reference genomes (Figure S5). We subsequently filtered for contigs
206 that aligned uniquely to either *P. syringae* and *P. rhizosphere* genomes and found
207 different k-mer coverage distributions in contigs aligning uniquely to each genome
208 (Figure S6), an observation that reinforced our confidence in the presence of the two
209 *Pseudomonas* species in this sample. Due to the high level of sequence divergence
210 between the *Pseudomonas* in our sample and the reference genomes present in the
211 database, it is difficult to assess typical deamination patterns in the dsDNA library
212 (Figure 2C). However, we were able to examine damage patterns in both *Pseudomonas*
213 species using the U-enriched fraction (Figure 2D), since the C-to-T signal is amplified
214 and is much higher than the basal level of substitutions.

215 In summary, we showed here that the U-selection method selectively enriches for
216 authentic microbial aDNA molecules in samples from plant and animal tissues with a
217 wide-distribution of ages and deamination levels. For instance, in *P. vagans*, U-selection
218 increases the fraction of molecules carrying a terminal C-to-T substitution at the 5'-end
219 2-3 fold over the library without enrichment, relative to the total number of molecules

220 sequenced. We think that the application of U-selection for ancient microbiome research
221 will be particularly useful in both samples with minute levels of deamination, where the
222 nucleotide divergence between samples and reference genomes will obscure the
223 identification of the C-to-T pattern typical of aDNA, as well as in moderately or heavily
224 deaminated samples which carry modern contaminants, since in those samples ancient
225 taxa would be efficiently enriched. Since it is extremely difficult to differentiate between
226 ante-mortem and early post-mortem colonizers based only on deamination patterns, it is
227 fundamental to also evaluate the biological relevance of detected taxa by comparing
228 them with reference modern microbiomes.

229 **Materials and Methods**

230 **Plant Samples**

231 We used herbarium specimens from three different plant species (*Arabidopsis thaliana*,
232 *Solanum tuberosum*, and *Solanum lycopersicum*) with ages ranging from 41 to 279
233 years (Table 1). *S. tuberosum* herbarium specimens were documented to be infected by
234 *Phytophthora infestans* (6). We used also *Zea mays* archaeological remains excavated
235 in the Turkey Penn shelter in Utah, USA (24). The *Zea mays* samples were dated using
236 accelerator mass spectrometry and have ages ranging between 1852 and 1881 years
237 BP (Before Present) (Table 1). The sequencing data for these samples is available on
238 the European Nucleotide Archive under study number PRJEB30666.

239 **Neanderthal samples**

240 We used Neanderthal samples (Table 1) prepared by (15), which were sequenced
241 deeper for this study.

242 **DNA extraction and library preparation**

243 DNA from all herbarium specimens and plant archaeological remains was performed as
244 previously described (6).

245 For each plant sample two libraries were produced, one using a double-stranded library
246 preparation (19, 25) and the second using the single-stranded U-selection protocol (15)

247 without enzymatic removal of uracils (26).

248 **Sequencing and initial data processing**

249 Since the length of aDNA molecules is in most of the cases shorter than the read length
250 of the sequencing platform, it is possible that a fragment of the aDNA molecule is
251 sequenced by both the forward and reverse read, and also that a part of the adaptor is
252 sequenced (27). Therefore, it is recommended to merge sequences based on the
253 overlapping fraction sequenced by both forward and reverse reads (27). We remove
254 adaptors and merged sequences using the software leeHom with the “--ancientdna”
255 option (28). Putative chimeric sequences were flagged as failing quality.

256 **Mapping of sequenced reads to their host genome**

257 Merged reads were mapped as single-ended reads to their respective or most closely
258 relative genome: *Zea mays* (29), *Arabidopsis thaliana* (30, 31), *Solanum tuberosum*
259 (32), *Solanum lycopersicum* (33), *Homo sapiens* (Genome Reference Consortium
260 Human Build 37). The mapping was performed using BWA-MEM (version 0.7.10) with
261 default parameters, which includes a minimum length cutoff of 30 bp (34).

262 **Metagenomics assignment of sequenced reads**

263 Reads were aligned to the full non-redundant NCBI nucleotide collection (nt) database
264 (downloaded January 2015) using MALT (version 0.0.12, (35)) in BlastN mode. The
265 resulting RMA files were analyzed using MEGAN (version 5.11.3, (36)). The reads were

266 assigned to the NCBI taxonomy using a lowest common ancestor algorithm (36).

267 **Mapping of sequenced reads to microbial genomes**

268 Libraries were mapped to microbial reference genomes of interest, after the presence of
269 certain taxa was detected during metagenomic assignment. Specifically, the references
270 of *Streptosporangium roseum* (37), *Pseudomonas syringae* pv. *syringae* B728a (38),
271 *Pseudomonas rhizosphaerae* (39) and *Pantoea vagans* (23) were used. Since mapping
272 metagenomic libraries to bacterial reference genomes is very prone to false alignments,
273 we used a different mapping strategy for these genomes. The mappings were
274 performed with bowtie2 (version 2.2.4, (40)), with the settings “--score-min 'L,-0.3,-0.3'
275 --sensitive --end-to-end” to increase stringency.

276 **Assessment of nucleotide substitution patterns**

277 All types of nucleotide substitutions relative to the reference genome were calculated
278 per library using mapDamage 2.0 (v. 2.0.2–12, (41)). The percentages of C-to-T
279 substitutions at the 5' end were extracted from the output file 5pCtoT_freq.txt produced
280 by mapDamage.

281 ***Pantoea vagans* genomic variation**

282 In order to reduce the effect of aDNA-associated C-to-T substitutions on variant
283 discovery, we used exclusively the U-depleted fraction of libraries where *P. vagans* was
284 detected in the metagenomic screening. The libraries were mapped to the *P. vagans*

285 reference genome using BWA-MEM, to reduce reference bias and increase SNP
286 discovery. False alignments from the metagenomic libraries posed a lesser problem
287 here, as variants were ascertained based on modern material. Variants for historical
288 samples were called for both libraries together using the bcftools (version 1.8, (42))
289 utilities mpileup (“bcftools mpileup -q 1 -l -Ou -f \$REF \$IN1 \$IN2”) and call (“bcftools call
290 --ploidy 1 -m -O -z”). Additionally, 11 assemblies of different contiguity were downloaded
291 from NCBI (<https://www.ncbi.nlm.nih.gov/genome/genomes/2707>). These assemblies
292 were aligned to the reference genome using minimap2 (version 2.10-r764, (43)) and its
293 “asm20” parameter preset. Only strains with at least 80% reference coverage were kept
294 for subsequent analysis (9/11, average reference coverage: 91%). The pafutils utility,
295 which is distributed with minimap2, was used to call variants from these alignments, with
296 the parameter set “-l 2000 -L 5000”. All resulting VCF files from modern samples were
297 merged using bcftools’ merge utility with the parameter “--missing-to-ref”, assuming that
298 those positions not called by pafutils in any one sample were indeed reference calls.
299 The merged VCF from modern material was then merged with the VCF from the two
300 historical samples using bcftools (version 1.8, (42)), and filtered to include only full
301 information, biallelic SNPs. This approach discovers sites, which are segregating in
302 modern material, and have read data (be it reference, alternative or segregating sites) in
303 both historical samples. The resulting VCF file was loaded into R using vcfR (version
304 1.7.0, (44)), and a PCA was produced by converting the information into a genlight
305 object using adegenet (version 2.0.1, (45)) in R (version 3.3.3, (46)).

306 ***Pseudomonas* spp. assembly and evaluation**

307 To evaluate the presence of *Pseudomonas* spp. strains in a *Solanum tuberosum* historic
308 herbarium sample, we extracted from this library all reads that were taxonomically
309 assigned to the *Pseudomonas* genus or to inferior taxonomic levels within it. These
310 reads were then assembled using SPAdes (version 3.5.0) with default parameters (47).
311 The resulting contigs were filtered for a minimum length of 2Kb, which yielded 3,314
312 contigs with a total length of 16Mb. We used the lastz (version 1.03.66, (48)) and Circos
313 (version 0.64, (49)) interface of AliTV (50) to align these contigs to either the *P. syringae*
314 or *P. rhizosphaerae* reference genome. We were able to align 72% of contigs to either
315 one or both of these reference genomes in alignments of at least 1Kb. We then
316 extracted all contigs which had alignments of at least 10Kb in length and were unique to
317 one of the reference genomes. These sets of contigs were again aligned to their
318 corresponding reference using AliTV as described above. Additionally, we used these
319 uniquely aligning contigs to assess their average kmer coverage during the assembly,
320 as reported by SPAdes.

321 **Acknowledgements**

322 We thank Verena Schuenemann for help in the laboratory; Patricia Lang, Claudia S.
323 Burbano, members of the Research Group for Ancient Genomics and Evolution, and
324 specially Talia Karasov for input on data analysis and comments on the manuscript;
325 Janet Kelso for help with processing the raw sequencing data; Ivan Gusic, Zeljko Kucan,
326 Carles Lalueza-Fox, Marco de la Rasilla, Antonio Rosas, Pavao Rudan, Sandra Knapp,
327 Bruce Benz, Michael Blake, R.G. Matson, Bryn Dentinger, Anna Stalter, Robert Capers,
328 John Peter for providing samples. This work was funded by the Max Planck Society and
329 its Presidential Innovation Fund.

330 **References**

- 331 1. Poinar HN, Schwarz C, Qi J, Shapiro B, Macphee RDE, Buigues B, Tikhonov A,
332 Huson DH, Tomsho LP, Auch A, Rampp M, Miller W, Schuster SC. 2006.
333 Metagenomics to paleogenomics: large-scale sequencing of mammoth DNA.
334 Science 311:392–394.
- 335 2. Gutaker RM, Burbano HA. 2017. Reinforcing plant evolutionary genomics using
336 ancient DNA. Curr Opin Plant Biol 36:38–45.
- 337 3. Orlando L, Gilbert MTP, Willerslev E. 2015. Reconstructing ancient genomes and
338 epigenomes. Nat Rev Genet 16:395–408.
- 339 4. Warinner C, Herbig A, Mann A, Fellows Yates JA, Weiß CL, Burbano HA, Orlando
340 L, Krause J. 2017. A Robust Framework for Microbial Archaeology. Annu Rev
341 Genomics Hum Genet 18:321–356.
- 342 5. Bos KI, Schuenemann VJ, Golding GB, Burbano HA, Waglechner N, Coombes BK,
343 McPhee JB, DeWitte SN, Meyer M, Schmedes S, Wood J, Earn DJD, Herring DA,
344 Bauer P, Poinar HN, Krause J. 2011. A draft genome of *Yersinia pestis* from victims
345 of the Black Death. Nature 478:506–510.
- 346 6. Yoshida K, Schuenemann VJ, Cano LM, Pais M, Mishra B, Sharma R, Lanz C,
347 Martin FN, Kamoun S, Krause J, Thines M, Weigel D, Burbano HA. 2013. The rise
348 and fall of the *Phytophthora infestans* lineage that triggered the Irish potato famine.

- 349 Elife 2:e00731.
- 350 7. Adler CJ, Dobney K, Weyrich LS, Kaidonis J, Walker AW, Haak W, Bradshaw CJA,
351 Townsend G, Soltysiak A, Alt KW, Parkhill J, Cooper A. 2013. Sequencing ancient
352 calcified dental plaque shows changes in oral microbiota with dietary shifts of the
353 Neolithic and Industrial revolutions. *Nat Genet* 45:450–5, 455e1.
- 354 8. Warinner C, Rodrigues JFM, Vyas R, Trachsel C, Shved N, Grossmann J, Radini A,
355 Hancock Y, Tito RY, Fiddyment S, Speller C, Hendy J, Charlton S, Luder HU,
356 Salazar-García DC, Eppler E, Seiler R, Hansen LH, Castruita JAS,
357 Barkow-Oesterreicher S, Teoh KY, Kelstrup CD, Olsen JV, Nanni P, Kawai T,
358 Willerslev E, von Mering C, Lewis CM Jr, Collins MJ, Gilbert MTP, Rühli F,
359 Cappellini E. 2014. Pathogens and host immunity in the ancient human oral cavity.
360 *Nat Genet* 46:336–344.
- 361 9. Weyrich LS, Duchene S, Soubrier J, Arriola L, Llamas B, Breen J, Morris AG, Alt
362 KW, Caramelli D, Dresely V, Farrell M, Farrer AG, Francken M, Gully N, Haak W,
363 Hardy K, Harvati K, Held P, Holmes EC, Kaidonis J, Lalueza-Fox C, de la Rasilla M,
364 Rosas A, Semal P, Soltysiak A, Townsend G, Usai D, Wahl J, Huson DH, Dobney
365 K, Cooper A. 2017. Neanderthal behaviour, diet, and disease inferred from ancient
366 DNA in dental calculus. *Nature*.
- 367 10. Boast AP, Weyrich LS, Wood JR, Metcalf JL, Knight R, Cooper A. 2018. Coprolites
368 reveal ecological interactions lost with the extinction of New Zealand birds. *Proc*

- 369 Natl Acad Sci U S A 115:1546–1551.
- 370 11. Briggs AW, Stenzel U, Johnson PLF, Green RE, Kelso J, Prüfer K, Meyer M, Krause
371 J, Ronan MT, Lachmann M, Pääbo S. 2007. Patterns of damage in genomic DNA
372 sequences from a Neandertal. *Proceedings of the National Academy of Sciences*
373 104:14616–14621.
- 374 12. Krause J, Briggs AW, Kircher M, Maricic T, Zwyns N, Derevianko A, Pääbo S. 2010.
375 A Complete mtDNA Genome of an Early Modern Human from Kostenki, Russia.
376 *Curr Biol* 20:231–236.
- 377 13. Prüfer K, Meyer M. 2015. Comment on “Late Pleistocene human skeleton and
378 mtDNA link Paleoamericans and modern Native Americans.” *Science* 347:835–835.
- 379 14. Weiß CL, Dannemann M, Prüfer K, Burbano HA. 2015. Contesting the presence of
380 wheat in the British Isles 8,000 years ago by assessing ancient DNA authenticity
381 from low-coverage data. *Elife* 4.
- 382 15. Gansauge M-T, Meyer M. 2014. Selective enrichment of damaged DNA molecules
383 for ancient genome sequencing. *Genome Res* 24:1543–1549.
- 384 16. Skoglund P, Malmström H, Raghavan M, Storå J, Hall P, Willerslev E, Gilbert MTP,
385 Götherström A, Jakobsson M. 2012. Origins and genetic legacy of Neolithic farmers
386 and hunter-gatherers in Europe. *Science* 336:466–469.

- 387 17. Meyer M, Fu Q, Aximu-Petri A, Glocke I, Nickel B, Arsuaga J-L, Martínez I, Gracia
388 A, de Castro JMB, Carbonell E, Pääbo S. 2014. A mitochondrial genome sequence
389 of a hominin from Sima de los Huesos. *Nature* 505:403–406.
- 390 18. Zaremba-Niedźwiedzka K, Andersson SGE. 2013. No ancient DNA damage in
391 Actinobacteria from the Neanderthal bone. *PLoS One* 8:e62799.
- 392 19. Meyer M, Kircher M. 2010. Illumina sequencing library preparation for highly
393 multiplexed target capture and sequencing. *Cold Spring Harb Protoc*
394 2010:db.prot5448.
- 395 20. Weiß CL, Schuenemann VJ, Devos J, Shirsekar G, Reiter E, Gould BA,
396 Stinchcombe JR, Krause J, Burbano HA. 2016. Temporal patterns of damage and
397 decay kinetics of DNA retrieved from plant herbarium specimens. *R Soc Open Sci*
398 3:160239.
- 399 21. Gansauge M-T, Meyer M. 2013. Single-stranded DNA library preparation for the
400 sequencing of ancient or damaged DNA. *Nat Protoc* 8:737–748.
- 401 22. Gansauge M-T, Gerber T, Glocke I, Korlević P, Lippik L, Nagel S, Riehl LM, Schmidt
402 A, Meyer M. 2017. Single-stranded DNA library preparation from highly degraded
403 DNA using T4 DNA ligase. *Nucleic Acids Res.*
- 404 23. Smits THM, Rezzonico F, Kamber T, Goesmann A, Ishimaru CA, Stockwell VO,
405 Frey JE, Duffy B. 2010. Genome sequence of the biocontrol agent *Pantoea vagans*

- 406 strain C9-1. *J Bacteriol* 192:6486–6487.
- 407 24. Matson RG, Chisholm B. 1991. Basketmaker II Subsistence: Carbon Isotopes and
408 Other Dietary Indicators from Cedar Mesa, Utah. *Am Antiq* 56:444–459.
- 409 25. Kircher M, Sawyer S, Meyer M. 2012. Double indexing overcomes inaccuracies in
410 multiplex sequencing on the Illumina platform. *Nucleic Acids Res* 40:e3.
- 411 26. Briggs AW, Stenzel U, Meyer M, Krause J, Kircher M, Pääbo S. 2010. Removal of
412 deaminated cytosines and detection of in vivo methylation in ancient DNA. *Nucleic
413 Acids Res* 38:e87.
- 414 27. Kircher M. 2012. Analysis of high-throughput ancient DNA sequencing data.
415 *Methods Mol Biol* 840:197–228.
- 416 28. Renaud G, Stenzel U, Kelso J. 2014. leeHom: adaptor trimming and merging for
417 Illumina sequencing reads. *Nucleic Acids Res* 42:e141.
- 418 29. Schnable PS, Ware D, Fulton RS, Stein JC, Wei F, Pasternak S, Liang C, Zhang J,
419 Fulton L, Graves TA, Minx P, Reily AD, Courtney L, Kruchowski SS, Tomlinson C,
420 Strong C, Delehaunty K, Fronick C, Courtney B, Rock SM, Belter E, Du F, Kim K,
421 Abbott RM, Cotton M, Levy A, Marchetto P, Ochoa K, Jackson SM, Gillam B, Chen
422 W, Yan L, Higginbotham J, Cardenas M, Waligorski J, Applebaum E, Phelps L,
423 Falcone J, Kanchi K, Thane T, Scimone A, Thane N, Henke J, Wang T, Ruppert J,
424 Shah N, Rotter K, Hodges J, Ingenthron E, Cordes M, Kohlberg S, Sgro J, Delgado

- 425 B, Mead K, Chinwalla A, Leonard S, Crouse K, Collura K, Kudrna D, Currie J, He R,
426 Angelova A, Rajasekar S, Mueller T, Lomeli R, Scara G, Ko A, Delaney K,
427 Wissotski M, Lopez G, Campos D, Braidotti M, Ashley E, Golser W, Kim H, Lee S,
428 Lin J, Dujmic Z, Kim W, Talag J, Zuccolo A, Fan C, Sebastian A, Kramer M, Spiegel
429 L, Nascimento L, Zutavern T, Miller B, Ambroise C, Muller S, Spooner W,
430 Narechania A, Ren L, Wei S, Kumari S, Faga B, Levy MJ, McMahan L, Van Buren
431 P, Vaughn MW, Ying K, Yeh C-T, Emrich SJ, Jia Y, Kalyanaraman A, Hsia A-P,
432 Barbazuk WB, Baucom RS, Brutnell TP, Carpita NC, Chaparro C, Chia J-M,
433 Deragon J-M, Estill JC, Fu Y, Jeddelloh JA, Han Y, Lee H, Li P, Lisch DR, Liu S, Liu
434 Z, Nagel DH, McCann MC, SanMiguel P, Myers AM, Nettleton D, Nguyen J,
435 Penning BW, Ponnala L, Schneider KL, Schwartz DC, Sharma A, Soderlund C,
436 Springer NM, Sun Q, Wang H, Waterman M, Westerman R, Wolfgruber TK, Yang L,
437 Yu Y, Zhang L, Zhou S, Zhu Q, Bennetzen JL, Dawe RK, Jiang J, Jiang N, Presting
438 GG, Wessler SR, Aluru S, Martienssen RA, Clifton SW, McCombie WR, Wing RA,
439 Wilson RK. 2009. The B73 maize genome: complexity, diversity, and dynamics.
440 *Science* 326:1112–1115.
- 441 30. Arabidopsis Genome Initiative. 2000. Analysis of the genome sequence of the
442 flowering plant *Arabidopsis thaliana*. *Nature* 408:796–815.
- 443 31. Swarbreck D, Wilks C, Lamesch P, Berardini TZ, Garcia-Hernandez M, Foerster H,
444 Li D, Meyer T, Muller R, Ploetz L, Radenbaugh A, Singh S, Swing V, Tissier C,
445 Zhang P, Huala E. 2008. The Arabidopsis Information Resource (TAIR): gene

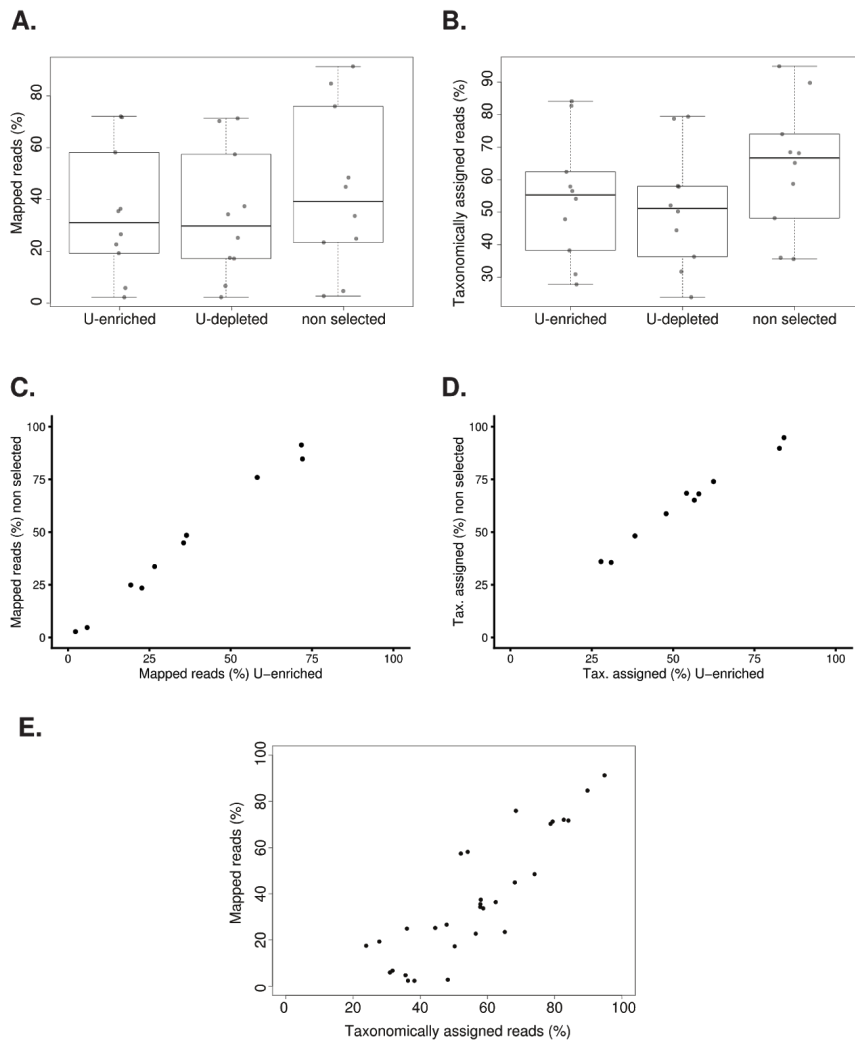
- 446 structure and function annotation. *Nucleic Acids Res* 36:D1009–14.
- 447 32. Potato Genome Sequencing Consortium, Xu X, Pan S, Cheng S, Zhang B, Mu D,
448 Ni P, Zhang G, Yang S, Li R, Wang J, Orjeda G, Guzman F, Torres M, Lozano R,
449 Ponce O, Martinez D, De la Cruz G, Chakrabarti SK, Patil VU, Skryabin KG,
450 Kuznetsov BB, Ravin NV, Kolganova TV, Beletsky AV, Mardanov AV, Di Genova A,
451 Bolser DM, Martin DMA, Li G, Yang Y, Kuang H, Hu Q, Xiong X, Bishop GJ,
452 Sagredo B, Mejía N, Zagorski W, Gromadka R, Gawor J, Szczesny P, Huang S,
453 Zhang Z, Liang C, He J, Li Y, He Y, Xu J, Zhang Y, Xie B, Du Y, Qu D, Bonierbale M,
454 Ghislain M, Herrera M del R, Giuliano G, Pietrella M, Perrotta G, Facella P, O'Brien
455 K, Feingold SE, Barreiro LE, Massa GA, Diambra L, Whitty BR, Vaillancourt B, Lin
456 H, Massa AN, Geoffroy M, Lundback S, DellaPenna D, Buell CR, Sharma SK,
457 Marshall DF, Waugh R, Bryan GJ, Destefanis M, Nagy I, Milbourne D, Thomson SJ,
458 Fiers M, Jacobs JME, Nielsen KL, Sønderkær M, Iovene M, Torres GA, Jiang J,
459 Veilleux RE, Bachem CWB, de Boer J, Borm T, Kloosterman B, van Eck H, Datema
460 E, Hekkert B te L, Goverse A, van Ham RCHJ, Visser RGF. 2011. Genome
461 sequence and analysis of the tuber crop potato. *Nature* 475:189–195.
- 462 33. Tomato Genome Consortium. 2012. The tomato genome sequence provides
463 insights into fleshy fruit evolution. *Nature* 485:635–641.
- 464 34. Li H. 2013. Aligning sequence reads, clone sequences and assembly contigs with
465 BWA-MEM. arXiv [q-bioGN].

- 466 35. Herbig A, Maixner F, Bos KI, Zink A, Krause J, Huson DH. 2016. MALT: Fast
467 alignment and analysis of metagenomic DNA sequence data applied to the
468 Tyrolean Iceman. bioRxiv.
- 469 36. Huson DH, Auch AF, Qi J, Schuster SC. 2007. MEGAN analysis of metagenomic
470 data. *Genome Res* 17:377–386.
- 471 37. Nolan M, Sikorski J, Jando M, Lucas S, Lapidus A, Del Rio TG, Chen F, Tice H,
472 Pitluck S, Cheng J-F, Others. 2010. Complete genome sequence of
473 *Streptosporangium roseum* type strain (NI 9100 T). *Stand Genomic Sci* 2:29.
- 474 38. Feil H, Feil WS, Chain P, Larimer F, DiBartolo G, Copeland A, Lykidis A, Trong S,
475 Nolan M, Goltsman E, Thiel J, Malfatti S, Loper JE, Lapidus A, Detter JC, Land M,
476 Richardson PM, Kyrpides NC, Ivanova N, Lindow SE. 2005. Comparison of the
477 complete genome sequences of *Pseudomonas syringae* pv. *syringae* B728a and
478 pv. *tomato* DC3000. *Proc Natl Acad Sci U S A* 102:11064–11069.
- 479 39. Kwak Y, Jung BK, Shin J-H. 2015. Complete genome sequence of *Pseudomonas*
480 *rhizosphaerae* IH5 T (= DSM 16299 T), a phosphate-solubilizing rhizobacterium for
481 bacterial biofertilizer. *J Biotechnol* 193:137–138.
- 482 40. Langmead B, Salzberg SL. 2012. Fast gapped-read alignment with Bowtie 2. *Nat*
483 *Methods* 9:357–359.
- 484 41. Jónsson H, Ginolhac A, Schubert M, Johnson PLF, Orlando L. 2013.

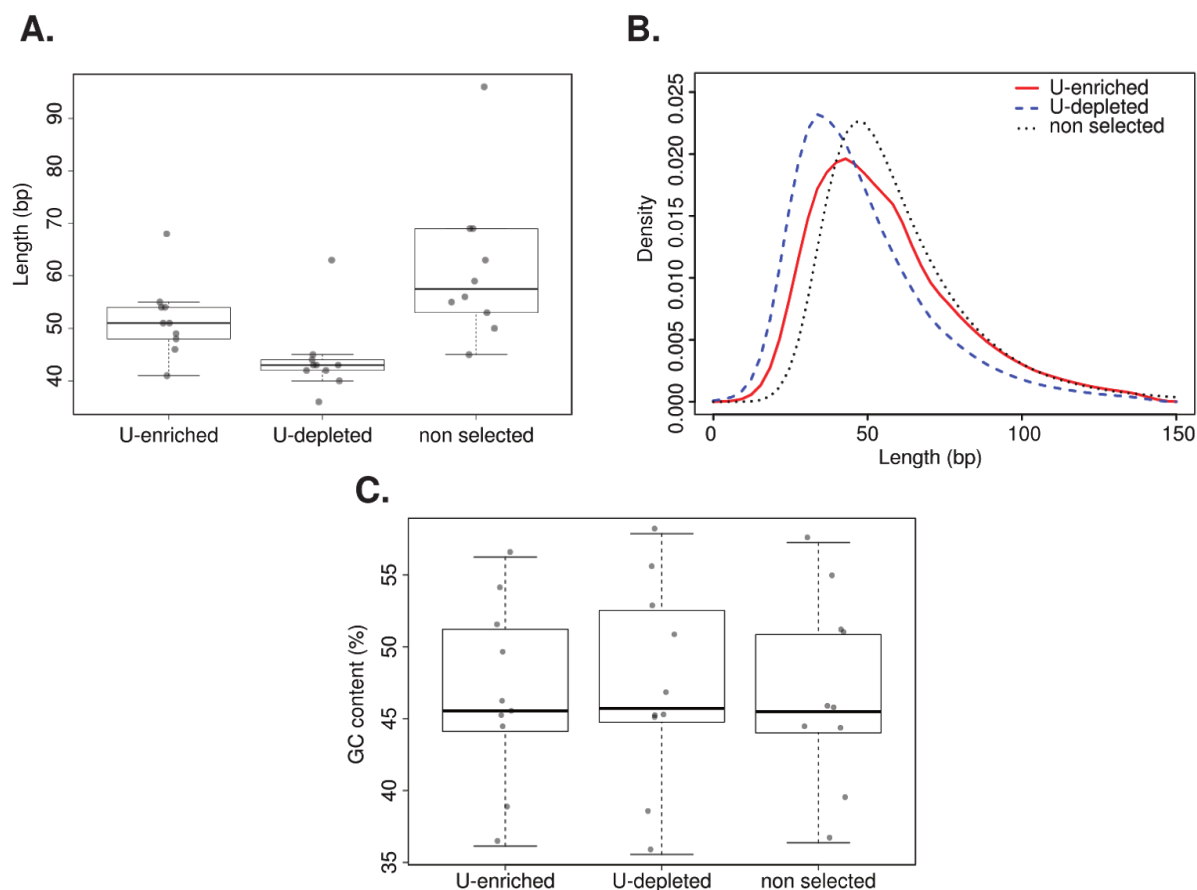
- 485 mapDamage2.0: fast approximate Bayesian estimates of ancient DNA damage
486 parameters. *Bioinformatics* 29:1682–1684.
- 487 42. Li H. 2011. A statistical framework for SNP calling, mutation discovery, association
488 mapping and population genetical parameter estimation from sequencing data.
489 *Bioinformatics* 27:2987–2993.
- 490 43. Li H. 2018. Minimap2: pairwise alignment for nucleotide sequences. *Bioinformatics*.
- 491 44. Knaus BJ, Grünwald NJ. 2017. vcfr: a package to manipulate and visualize variant
492 call format data in R. *Mol Ecol Resour* 17:44–53.
- 493 45. Jombart T, Ahmed I. 2011. adegenet 1.3-1: new tools for the analysis of
494 genome-wide SNP data. *Bioinformatics* 27:3070–3071.
- 495 46. R Development Core Team. 2008. R: A Language and Environment for Statistical
496 Computing. R Foundation for Statistical Computing, Vienna, Austria.
- 497 47. Bankevich A, Nurk S, Antipov D, Gurevich AA, Dvorkin M, Kulikov AS, Lesin VM,
498 Nikolenko SI, Pham S, Prjibelski AD, Pyshkin AV, Sirotkin AV, Vyahhi N, Tesler G,
499 Alekseyev MA, Pevzner PA. 2012. SPAdes: a new genome assembly algorithm and
500 its applications to single-cell sequencing. *J Comput Biol* 19:455–477.
- 501 48. Harris RS. 2007. Improved pairwise alignment of genomic DNA. The Pennsylvania
502 State University.

- 503 49. Krzywinski M, Schein J, Birol I, Connors J, Gascoyne R, Horsman D, Jones SJ,
504 Marra MA. 2009. Circos: an information aesthetic for comparative genomics.
505 Genome Res 19:1639–1645.
- 506 50. Hohlfeld S, Ankenbrand M, Förster F, Hackl T. 2016. AliTV: Version 0.4.1. Zenodo.

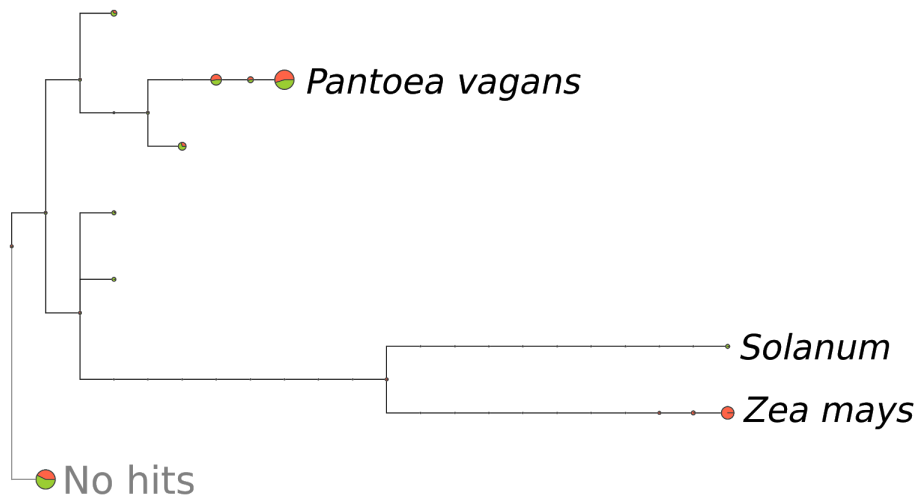
507 **Supplementary Figures**



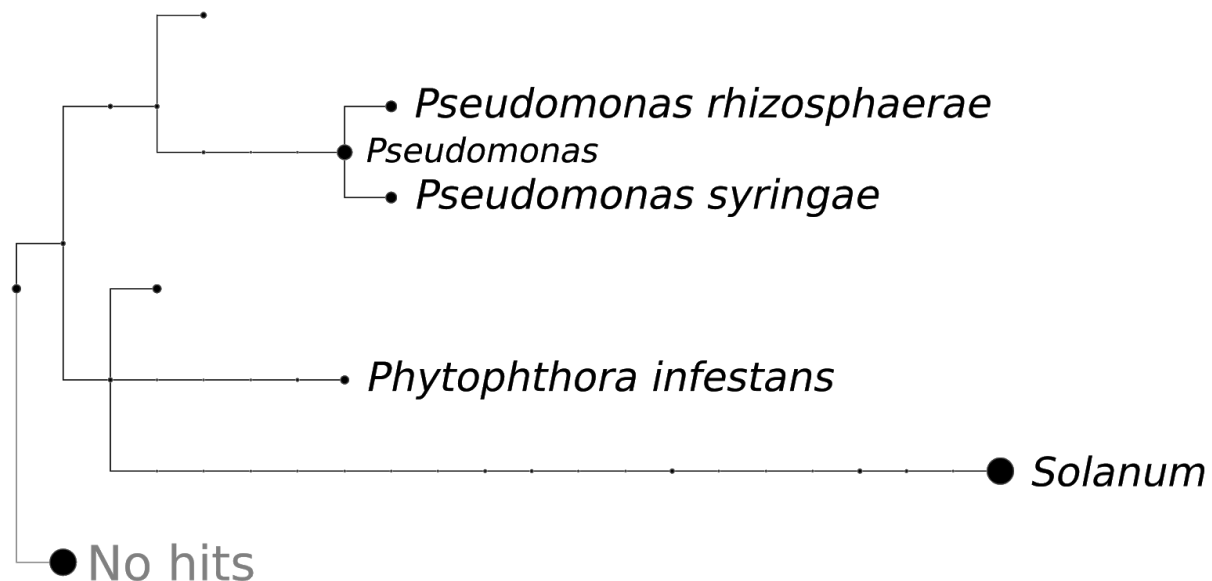
508 **Figure S1.** Mapped and taxonomically assigned reads of plant historical specimens. **A.**
509 Distributions of percentage of mapped reads for non-selected and U-selected libraries
510 (U-enriched and U-depleted fractions). **B.** Distributions of percentage of taxonomically
511 assigned reads for non-selected and U-selected libraries (U-enriched and U-depleted
512 fractions). **C.** Correlation of the percentage of mapped reads between the U-enriched
513 and the non-selected library **D.** Correlation of the percentage of taxonomically assigned
514 reads between the U-enriched and the non-selected library **E.** Relation between
515 percentages of mapped and taxonomically assigned reads from U-selected libraries
516 (U-enriched fraction).



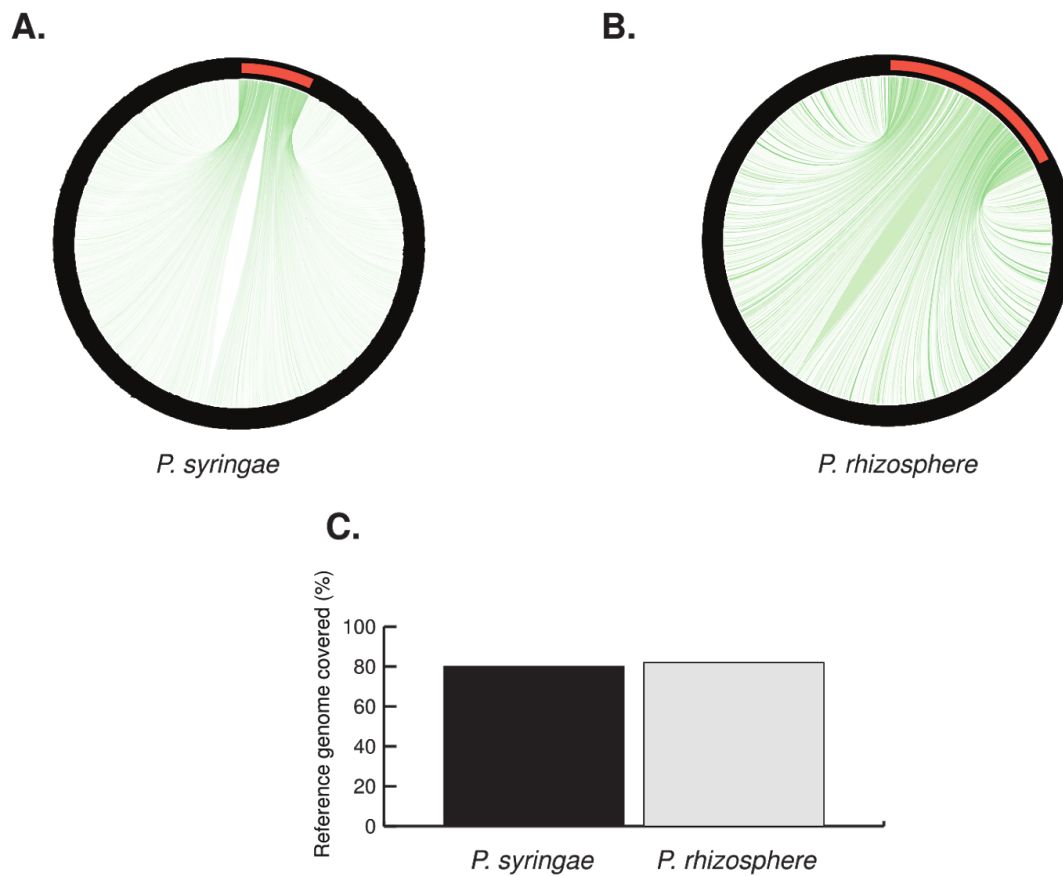
517 **Figure S2.** Length and GC content of plant historical specimens. **A.** Distributions of
518 mean length for non-selected and U-selected libraries (U-enriched and U-depleted
519 fractions). Median values are denoted as black lines and points show the original value
520 for each individual sample. **B.** Length distribution of *Arabidopsis thaliana* sample
521 NY1365375 for a non-selected and U-selected library (U-enriched and U-depleted
522 fractions). **C.** Distributions of mean GC content for non-selected and U-selected libraries
523 (U-enriched and U-depleted fractions).



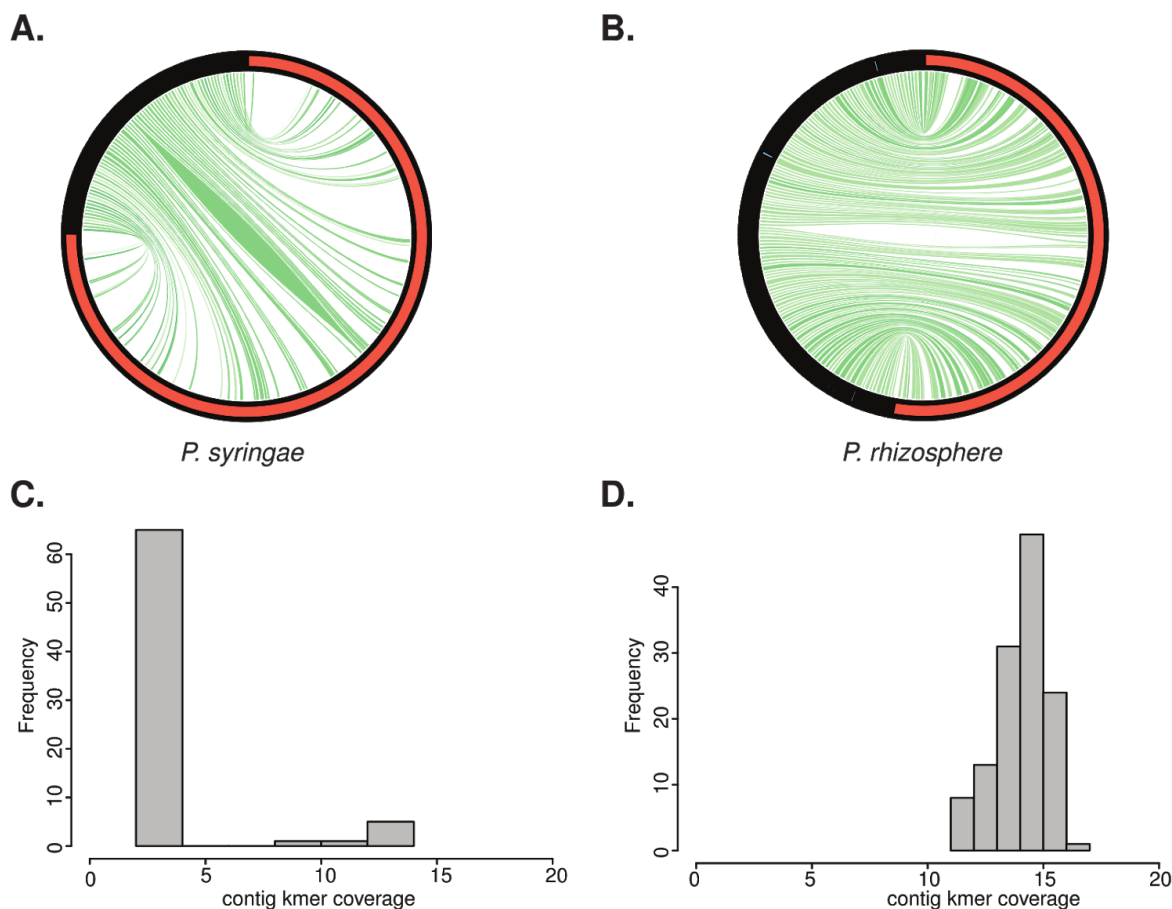
524 **Figure S3.** Taxonomic tree of reads from *Solanum tuberosum* and *Zea mays* assigned
525 to different taxonomic levels. The size of the circle represents the amount of reads
526 assigned to a particular part or the taxonomy. *S. tuberosum*- and *Z. mays*-derived reads
527 are shown in green and orange, respectively.



528 **Figure S4.** Taxonomic tree of reads from a *Solanum tuberosum* library assigned to
529 different taxonomic levels. The size of the circle represents the amount of reads
530 assigned to a particular part of the taxonomy. Reads assigned to some species
531 *Phytophthora infestans*, *Pseudomonas syringae* and *Pseudomonas rhizosphere*, as well
532 as the genera *Pseudomonas* and *Solanum* are named in the taxonomic tree.



533 **Figure S5.** De novo assembly and genomic coverage of *Pseudomonas syringae* and
534 *Pseudomonas rhizosphere* from a *Solanum tuberosum* sample. **A.** Alignments
535 (represented as green lines) between all de novo assembly contigs (black) and *P.*
536 *syringae* reference genome (red). **B.** Alignments (represented as green lines) between
537 all de novo assembly contigs (black) and *P. rhizosphere* reference genome (red). **C.**
538 Percentage of reference genome of *P. syringae* and *P. rhizosphere* covered by de novo
539 assembled contigs from A. and B., respectively.



540 **Figure S6.** De novo assembly (uniquely mapped contigs) and contig k-mer coverage of
541 *Pseudomonas syringae* and *Pseudomonas rhizosphere* from a *Solanum tuberosum*
542 sample. **A.** Alignments (represented as green lines) between de novo assembly contigs
543 (black) uniquely mapped to *P. syringae* reference genome (red). **B.** Alignments
544 (represented as green lines) between de novo assembly contigs (black) uniquely
545 mapped to *P. rhizosphere* reference genome (red). **C.** Histogram of contig k-mer
546 coverage from de novo assembled contigs uniquely mapping to *P. syringae*. **D.**
547 Histogram of contig k-mer coverage from de novo assembled contigs uniquely mapping
548 to *P. rhizosphere*.